LAWRENCE
LIVERMORE
NATIONAL
LABORATORY

UCRL-JRNL-219215

Depth Dependence of the Mechanical Properties of Human Enamel by Nanoindentation

Jikou Zhou, Luke L. Hsiung

February 22, 2006

Journal of Biomedical Materials Research Part A

Depth Dependence of the Mechanical Properties of Human Enamel by Nanoindentation

Jikou Zhou and Luke L. Hsiung

Lawrence Livermore National Laboratory, Livermore, CA 94551

Abstract

Nanoindentation has recently emerged to be the primary method to study the mechanical behavior and reliability of human enamel. Its hardness and elastic modulus were generally reported as average values with standard deviations that were calculated from the results of multiple nanoindentation tests. In such an approach, it is assumed that the mechanical properties of human enamel are constant, independent of testing parameters, like indent depth and loading rate. However, little is known if they affect the measurements. In this study, we investigated the dependence of the hardness and elastic modulus of human enamel on the indent depth. We found that in a depth range from 100 nm to 2000 nm the elastic moduli continuously decreased from ~ 104 GPa to ~ 70 GPa, and the hardnesses decreased from ~ 5.7 GPa to ~ 3.6 GPa. We then considered human enamel as a fiber-reinforced composite, and used the celebrated rule of mixture theory to quantify the upper and lower bounds of the elastic moduli, which were shown to cover the values measured in the current study and previous studies. Accordingly, we attributed the depth dependence of the hardness and modulus to the continuous microstructure evolution induced by nanoindenter.

Keywords: Enamel, Elastic modulus, Hardness, Nanoindentation, Composite

INTRODUCTION

Human enamel is an anisotropic composite, consisting of aligned prism rods with protein-rich sheath. Each prism rod contains multiple hydroxyapatite (HAP) single crystals (SCs) that are separated from each other by enamelin. The multiscale microstructure in cross section has been clearly revealed by Habletiz et al., [1] (cited in Figure 1 for convenient description). As the hardest tissue in the human body, the enamel coating on teeth makes it possible to cut, tear, and grind food. The mechanical behavior and reliability of enamel have been major concerns in numerous studies since 1958 [2]. In most of the early studies, the fracture toughness, elastic modulus, and strength were measured using flexural testing, compression testing [3-5], or microindentation testing [5-7]. Since instrumented nanoindenter became available in the 1990s, it has become the predominant method to study enamel's mechanical behavior [8-14]. In nanoindentation testing, both load and indent depth are continuously monitored and recorded, making it possible to simultaneously identify several important mechanical properties such as hardness, elastic modulus, fracture toughness, and friction properties. The nanoindentation testing, in conjunction with scanning probe microscopy (SPM), can also probe the mechanical properties of different phases or microstructural domains in human enamel [1,10,14].

Previous studies have reported the statistics (average values and standard deviations) of multiple measurements. Cuy et al. [8] measured hardnesses and elastic moduli by making indents in the axial section of maxillary second molars (M2). They established maps of hardness and elastic modulus that showed the regions closest to the occlusal surface have the highest values of hardness ($H > 6$ GPa) and elastic modulus ($E > 115$ GPa), while the regions near the dental-enamel junction (DEJ) have the lowest values ($H < 3$ GPa and $E < 70$ GPa). Jiang et al. [9] found

a wide range of hardnesses (0.5 GPa < H <5.0 GPa) and moduli (10 GPa < E <80 GPa) also by making indents in the axial section. Their results suggested that the hardness and elastic moduli exponentially increased as the degree of alignment of the prisms increased.

Nanoindention tests were also carried out in the occlusal section [1,6,10,14]. Habelitz et al. [1] found that the hardness measured in the occlusal section was higher than in the axial section. They also found that the hardness and elastic modulus of the inter-rod organic sheath phase (E: 86.4 ± 11.7 GPa and H: 3.9 ± 0.4 GPa) were similar to those of the prisms. This is contrary to the results reported by Ge et al. [10], who found that prisms were about 2-3 times harder than the inter-rod organic phase.

The wide ranges in the published data were generally attributed to variations in the microstructure or microchemistry of human enamel. Cuy et al. [8] attributed the variations in hardnesses and elastic moduli to constituent gradients of HAP crystals (calcium and phosphate salt) from the occlusal surface to DEJ. Jiang et al. [9] correlated the modulus and hardness values to the degree of alignment of the prism rods. It has also been suggested that the hardness and modulus values vary depending on water content in enamel [15]. Despite the importance of these factors, any one or combination of them cannot provide a convincing explanation for the significant discrepancies in measurements.

On the other hand, the nanoindentation testing measures the mechanical response of the materials in the local region to the concentrated load applied through the tiny indenter [16]. If the material being tested has a varying microstructure, or the microstructure evolves as the indentation testing proceeds, the measured properties may also change with depth. This phenomenon has often been observed in crystalline materials [17]. In this sense, each single nanoindentation test actually measures the properties of the enamel corresponding to a certain

depth or load level, because the hardness and elastic modulus values were measured using a portion of the unloading curve or by measuring the residual size of the indent. However, little is known about whether the enamel's properties change with increasing depth and load level.

The objective of this work is to study the potential variations of the hardness and elastic modulus of enamel with increasing indent depth. A continuous stiffness measurement (CSM, developed by MTS Nano Instrument®) technique was used to measure the hardness and elastic modulus values in a depth range from 100 nm to 2000 nm. The results were then evaluated and combined with previous studies using the famous rule of mixture that was derived to predict the properties and design the structure of composites. The effects of indent depth on the hardness and elastic modulus measurements were then attributed to the microstructural evolution of enamel induced by the nanoindenter.

MATERIALS AND METHOD

As mentioned earlier, human enamel consists of aligned prisms in the organic matrix. In the region near the occlusal surface, the prisms are oriented in a direction perpendicular to the occlusal surface [8]. However, human teeth, especially molars, generally have a concave occlusal surface with varying curvatures. The prisms may not be perpendicular to the surface prepared for testing if the intact occlusal surface has been ground or polished. The inclined angle between the prisms and the specimen surface may affect the mechanical response to the indentation loading, because the load is applied in a direction normal to the specimen surface [9]. To minimize this effect, the enamel of a second molar was dissected into small pieces about 2 mm wide and 1 mm thick with relatively flat surfaces so that all prisms near the occlusal surface could be reasonably

assumed uniformly perpendicular to the surface prepared for testing. All the small enamel pieces were stored in air for at least one week to reach a stable dry condition. According to previous studies [1,15], the absolute hardness and elastic modulus values obtained from dry samples may be slightly higher than those from wet samples. This is expected for all tests and, therefore, will not affect the trend of the data.

After grinding and polishing, nanoindentation testing was carried out using an MTS XP® nanoindenter (MTS Nano Instrument, Oak Ridge, TN). Each test consisted of three segments: the loading segment, the peak load holding segment, and the unloading segment. The indent depth corresponding to the last point of loading segment in a test is defined as the maximum indent depth (MID). Since human enamel contains organic matrix phase with a mechanical behavior sensitive to strain rate, special efforts were made to ensure the material was loaded at a constant strain rate (CSR). A target CSR (t-CSR) of 0.05 s^{-1} was set for the loading segments of all tests. The hardnesses and elastic moduli were measured using a continuous stiffness measurement (CSM) technique, which involves applying a very small oscillation force to the loading force at high frequency. From the oscillation of the resulting depth signals one can continuously measure the unloading stiffness and calculate the hardness and modulus values during the loading segment [17,18]. The amplitude of the force oscillation is small enough that it does not affect the deformation process. A three-sided Berkovich diamond tip was used in this study. Before the testing, both the tip and the nanoindenter were calibrated using fused silica and single crystal aluminum.

After nanoindentation, the indents were examined using a scanning electron microscopy (SEM). This was done to check possible pileups and cracks that may be generated during

nanoindentation testing. SEM was operated at low voltages so that no conductive coating was required to ensure that no cracks would be covered and become invisible.

RESULTS

Preliminary nanoindentation tests showed that a load of ~ 300 mN was required to make indents about 2000 nm deep. This load level is close to the loading capacity of the nanoindenter. Hence, 2000 nm was set up as the MID for the first set of tests. A typical load-depth curve is shown in Figure 2. It is well known that the strain rate ($\dot{\varepsilon}$) of indentation loading is generally calculated using the relationship, $\dot{\varepsilon} = \dot{h}/h$, in which h is the indent depth [18]. The computed strain rate corresponding to the load-depth curve with MID equal to 2000 nm (Figure 2) is shown in Figure 3a. One important characteristic of this curve is that a ramping stage was needed to reach a CSR. During this stage, the tip penetrated the surface ~ 500 nm deep. This depth is accordingly defined as the ramping depth. During the ramping stage, the strain rates dramatically changed (Figure 3a), and the elastic moduli continuously increased from very low values (~ 30 GPa) to a peak level (~ 90 GPa). This was followed by a gradual decrease as the depth increased. At the maximum depth of 2000 nm, the elastic modulus reached a value of about 70 GPa. Multiple indentation tests were carried out using the same maximum depth of 2000 nm and the same t-CSR of 0.05 s^{-1}; the modulus-depth curves are presented in Figure 4a. All curves exhibit the same features and trends. The elastic moduli at each indent depth are also very close, suggesting that the results are consistent and systematic.

It is noted that there were three displacement bursts in the loading segment (Figure 2). Each burst caused the strain rate to rise momentarily, but it receded to the constant value shortly

after the burst (Figure 3a). Since these bursts do not affect the measurements and the subsequent analysis, they will not be further mentioned in this study.

The anomalous increase of the elastic modulus in the ramping stage may be associated with two possible reasons. The first is the changing strain rates. Human enamel contains protein-rich matrix with a viscoelastic behavior that is sensitive to strain rates. Since the indentation deformation in the ramping stage proceeded under changing strain rates, the measurements may therefore be affected. Secondly, the surface layer of the specimen may have been softened during the sample preparing procedure. In an effort to understand which of these reasons is more likely to be true, we carried out a second set of tests, using 500 nm as the maximum depth and choosing the same target CSR of 0.05 s^{-1}. One of the typical load-depth curves is shown in Figure 2 for comparison. The corresponding strain rates were computed and are presented in Figure 3b. A similar ramping stage was observed. The ramping depth is about ~ 100 nm. This is much smaller than the 500 nm required for the deeper indents in the first set of tests (Figure 3a).

The modulus-depth curves of the second set of tests exhibit similar characteristics to those from the first set of tests (Figure 4a). The modulus values continuously rose to peak levels of about 104 GPa. As loading proceeded, the elastic modulus values gradually decreased to an average value of ~ 91 GPa at a depth around 500 nm. This value is almost the same as the peak levels of the elastic modulus (~ 89 GPa) measured in the first set of tests. The same decreasing trend exhibited by the elastic moduli measured in the two sets of tests becomes more evident with a superposed trendline in Figure 4a. It is indicative that the rising elastic moduli within the ramping stages were not caused by surface softening. Instead, they are associated with the significantly changing strain rates. Accordingly, we excluded the rising portions of the curves, and only data from the deceasing portions will be considered and discussed further.

With this in mind, the multiple curves of the two sets of tests can be unified by extracting data from the decreasing portions. These are shown in Figure 4b, in which each data point represents the average value and the standard deviation of all the data points falling within a small depth range centered in the same depth in Figure 4a. For instance, the point corresponding to 200 nm depth in Figure 4b was calculated from those data points falling within the depth range from 199 nm to 201 nm in Figure 4a. The combination of the two sets of data clearly shows that the elastic moduli of enamel systematically decrease with increasing indent depth.

The actual CSR (a-CSR) reached by the indents made in the two sets of tests are the same, as indicated by the shaded line in Figure 3a. However, the a-CSR was about 0.026 s^{-1}, which is less than the t-CSR of 0.05 s^{-1}. This suggests the same a-CSR can be reached provided the same t-CSR is used. The former is systematically lower than the latter. Furthermore, the ramping depths seem to be associated to the maximum depth. A smaller ramping depth is required when the maximum depth is also small.

The hardness curves are presented in Figure 5a, and treated in a similar way to elastic modulus. The statistics corresponding to each indent depth are shown in Figure 5b. Again, the combination of the two sets of tests shows the decreasing trend of hardness with increasing indention depth, although the hardness values in the depth range between 400 nm and 500 nm are fairly different for the two sets of tests.

Cracks were observed around some of the indents. Most of them were initiated at the indent corners (Figure 6a). But they are not necessarily associated with deeper indents. For example, cracks were observed in a small indent corresponding to a test with a maximum depth of 500 nm (Figure 6a) while no cracks were observed in a deeper indent (Figure 6b) corresponding to a test with a maximum depth of 2000 nm. Based on this observation, we

believe that cracks may be produced during loading, but not always. The measured hardness and modulus values are not significantly affected by crack initiation and growth. Moreover, there is no significant observable pileup, and regarding it no further discussion will be made.

DISCUSSION

In recent years, nanoindentation has been increasingly used to study the mechanical properties of human enamel. The relevant results are summarized in Table 1. Most of these studies concentrated on the gradual change of mechanical properties across the axial section, especially across DEJ [7-9,12-14]. These studies reported wide ranges of hardnesses (0.5 GPa – 6 GPa) and elastic moduli (10GPA – 115 GPa). We will not discuss the data obtained from the axial section in this paper. Instead, we will focus on the hardness and modulus values that were measured in the occlusal section [1,10,11,14]. The previous studies reported the average values and standard deviations of multiple measurements. Some careful authors even reported the maximum depths or loads that were used to make indents (Table 1). The elastic modulus measured by Fong et al [14] was 98.3 ± 5.9 GPa using a maximum indent depth of about 100 nm. Habelitz et al. [1] reported that the elastic modulus was 87.5 ± 2.2 GPa when the maximum depth was about 300 nm. In a recent study by Ge et al. [10], the elastic moduli of the prism and the inter-rod organic sheath were 83.4 ± 7.1 GPa and 39.5 ± 4.1 GPa, respectively. However, no explicit indent depth values were provided in this study. The results obtained by Habelitz et al. [1] and Fong et al. [14] are presented in Figure 4b. They are surprisingly consistent with the elastic moduli measured in the current study. They are also in harmony with the same decreasing trend obtained in this study, although their data are a little lower than our results. This may be

due to the different sample conditions: we used dry samples, while wet samples were used in the previous studies.

The mechanical properties measured using nanoindentation are strongly dependent on the mechanical response of the materials around the indenter, a response largely determined by the local microstructure [16]. Like many other biological materials, human enamel possesses a hierarchical structure. The first level consists of prism rods and the organic sheath. At the second level, each prism rod is composed of hydroxyapaptite single crystals oriented along the prism axis bonded together by the organic enamelin. The single HAP crystal is about 50 nm in diameter, and the thickness of enamelin is in nanometer scale. In the region close to the occlusal surface, both the single HAP crystals and the prism rods are oriented in a direction that is perpendicular to the surface [8]. It is, therefore, reasonable to consider the tested enamel as a unidirectional fiber reinforced composite [19,20]. The mechanical properties of such an orthotropic composite have an upper and lower bounds, corresponding to two extreme loading conditions as shown in Figures 7a and 7b, respectively [19]. In the first one (Figure 7a), a load is applied parallel to the reinforcement prisms. The strain in the organic matrix and reinforcement phase (HAP prisms) must be equal to keep them from sliding past each other. This leads to the constant-strain rule of mixture:

$$E_E = V_H E_H + V_P E_P \qquad (1)$$

where E is the elastic modulus, V is the volume fraction of the prism or protein-rich matrix; subscripts E, H and P refer to enamel, HAP crystals in prisms, and protein-rich matrix, respectively.

On the other hand, when a load is applied perpendicular to the reinforcement prisms as shown in Figure 7b, the stress in the crystal is equal to that in the surrounding organic phase. The overall strain is the sum in the two phases, resulting in a constant-stress rule of mixture:

$$\frac{1}{E_E} = \frac{V_H}{E_H} + \frac{V_P}{E_P} \tag{2a}$$

or

$$E_E = \frac{E_H E_P}{V_H E_H + V_P E_P} \tag{2b}$$

Equations 1 and 2 predict the upper and lower bound estimates of the elastic modulus of a composite, respectively. The above equations can be expressed in a general format [19]:

$$(X_E)^n = V_H (X_H)^n + V_P (X_P)^n \tag{3}$$

where X is a property such as elastic modulus, hardness, and other physical parameters, n is a number between +1 and -1, but not equal to 0. The value depends on the characteristics of the reinforcement phase. It also depends on the relative orientation between the loading axis and the HAP crystals. When n equals +1 or -1, Equation 3 reduces to Equation 1 or 2, respectively. When X represents the hardness, we obtain the similar upper and lower bounds for hardness, provided that the hardness values for the HAP crystalline phase and the organic phase are known.

According to Katz [21], the elastic modulus of HAP crystals is ~ 114 GPa, and the elastic modulus of keratin, 4.3 GPa, can be used for the organic phase. Inserting these values into Equations 1 and 2, the upper and lower bounds of the elastic modulus can be estimated over a range of volume fraction of HAP crystals. This is shown in Figure 8. The plot shows that the measured elastic modulus values should be a range dependent on the volume fraction of HAP crystals and the relative orientation between the load axis and crystalline rods. For instance, the

volume fraction of crystalline in the region of the occlusal surface is typically about 0.95 [8], so a possible range from ~ 60 GPa to ~ 108 GPa may be expected. The ranges of elastic modulus for varying volume fraction between 0.80 -1.00 are also indicted in Figure 8 as the shaded area. The ranges cover all the published results and the results of the current study. The above argument should also apply to the hardness of human enamel. Since there are no reliable strength data for the HAP crystals and organic phase, we cannot estimate the two bounds for hardness.

The dependent relationship between hardness and indent depth is a common phenomenon in crystalline materials [22]. It is called *size effect*: i.e. smaller/shallower indents result in higher hardness values. Size effect is attributed to the geometrically necessary dislocations (GNDs) generated to accommodate the shape of the nanoindenter tip. The GNDs are added to background dislocations known as statistically stored dislocations (SSDs). The relative density fraction of GNDs increases with decreasing indent size, leading to rising strain hardness. A dislocation mechanism such as this is unlikely to operate in human enamel.

As mentioned before, the diameter of a HAP single crystal (SC) is about 50 nm, and the crystals are separated from each other by organic enamelin several nanometers thick. Dislocations in one crystal rod are incapable of accommodating deformation since the tip radius of the indenter is also about 50 nm—however, deformation may occur when the HAP SCs move and rotate. Hence, the dependence of hardness and elastic modulus on indent depth may be associated with the realignment of the HAP SCs induced by the indenter. When the tiny diamond tip is pushed into the occlusal section, one of the HAP SCs may be hit, pushed downward and outward, and deformed. At a small indent depth adjacent HAP SCs are not involved, as illustrated in Figure 9a. More HAP SCs become involved as penetration continues. The inclined angles between the pushing load P and the long axis of the HAP SCs, θ, increases continuously

with indent depth, as shown in Figures 9b-9c. This causes the loading condition to shift from a condition of constant-strain to constant-stress, i.e. from upper bound to lower bound values.

It should be noted that the schematics in Figure 9 are only conceptual illustrations. Each HAP SC in Figure 9 may represent a multitude. The HAP SCs may be broken and then realigned rather than deformed. Nevertheless, the realigned prisms are responsible for reducing hardness and modulus as indent depth increases. The above discussion is based on the fact that deformation is limited to a small volume around the indenter tip. The material far from the tip is not affected. There must be boundaries between the deformed and non-deformed regions. Future studies may be carried out to explore the evolution of the microstructure within the deformation region and the movement of the boundaries during testing. It would also be interesting to study the role of the interface between HAP single crystals and the surrounding organic phase [23].

This study is the first piece of work, to the authors' knowledge, that explores the depth dependence of the mechanical properties of enamel and the deformation behavior induced by a nanoindenter tip in nanoscale. We hope it serves as a seed for future studies. Such studies may establish quantitative relationships between microstructure evolution and property changes in nanoindentation testing, and provide new insights into the deformation and fracture of human enamel resulting from mastication.

CONCLUSIVE REMARKS

In this study, the effect of indent depth on the hardness and elastic modulus of human enamel has been unprecedentedly studied using a continuous stiffness measurement (CSM) technique. The significant results are summarized as follows.

1. The measured hardnesses or elastic moduli of enamel should be noted as a range with lower and upper bounds rather than as a single value. The bounds are determined by the volume fraction of the HAP crystals, while the measured values depend on the relative orientations between loading axis and aligned prism rods.
2. When measured by making indents in the occlusal section, both the hardness and elastic modulus values decrease with increasing indentation depth. In a depth range from 100 nm to 2000 nm, the elastic modulus decreases by 30% from ~ 104 GPa to ~ 70 GPa, and the hardness decreases by more than 30% from ~ 5.7 GPa to ~ 3.6 GPa.
3. Human enamel in the region close to the occlusal surface may be considered a unidirectional fiber reinforced composite. The depth effect can thus be attributed to the continuous change in microstructure induced by the nanoindenter tip. The famous rule of mixture theory was implemented in the process, which perfectly quantifies the lower and upper bounds of the elastic modulus measured in the occlusal section. Future studies may be carried out to investigate the evolution of microstructure during nanoindentation testing.

Acknowledgments

This work was performed under the auspices of the U. S. Department of Energy by the University of California, Lawrence Livermore National Laboratory under Contract No. W-7405-Eng-48. The authors gratefully acknowledge to Dr. Amy Mao for stimulating discussion and providing enamel specimens.

References:

1. Habelitz S, Marshall SJ, Marshall Jr GW and Balooch M. Mechanical properties of human dental enamel on the nanometer scale. Arch Oral Biol 2001; 46: 173–183.
2. Craig RG and Peyton FA. The microhardness of enamel and dentin. J Dent Res 1958; 37: 661-668.
3. El Mowafy OM and Watts DC. Fracture toughness of human dentin. J Dent Res 1986; 65: 677-681.
4. Rasmussen ST, Patchin RE, Scott DB and Heuer AH. Fracture properties of human enamel and dentin. J Dent Res 1976; 55: 154-164.
5. Craig RG, Peyton FA and Johnson DW. Compressive properties of enamel, dental cements, and gold. J Dent Res 1961; 40: 936-945.
6. Xu HHK, Smith DT, Jahanmir S, Romberg E, Kelly JR, Thompson VP and Rekow ED. Indentation damage and mechanical properties of human enamel and dentin. J. Dent Res 1998; 77: 472–480.
7. Imbeni V, Kruzic JJ, Marshall Jr GW, Marshall SJ and Ritchie RO. The dentin-enamel junction and the fracture of human teeth. Nature Materials 2005; 4: 229-232.
8. Cuy JL, Mann AB, Livi KJ, Teaford MF and Weihs TP. Nanoindentation mapping of the mechanical properties of human molar tooth enamel. Arch Oral Biol 2002; 47: 281–91.
9. Jiang H, Liu X-Y- Lim CT and Hsu CY. Ordering of self-assembled nanobiominerals in correlation to mechanical properties of hard tissues. Appl Phys Lett 2005; 86: 163901-163903.
10. Ge J, Cuia FZ, Wang XM and Feng HL. Property variations in the prism and the organic sheath within enamel by nanoindentation. Biomaterials 2005; 26: 3333–3339.
11. Finke M, Hughes JA, Parker DM and Jandt KD. Mechanical properties of in situ demineralised human enamel measured by AFM nanoindentation. Surf Sci 2001; 491: 456–467.
12. Mahoney E, Holt A, Swain M and Kilpatrick N. The hardness and modulus of elasticity of primary molar teeth: an ultra-micro-indentation study. J Dent 2000; 28: 589–594.
13. Willems G, Celis JP, Lambrechts P, Braem M and Vanherle G. Hardness and Young's modulus determined by nanoindentation technique of filler particles of dental restorative materials compared with human enamel. J Biomed Mater Res 1993; 27: 747–755.

14. Fong H, Sarikaya M, White SN and Snead ML. Nano-mechanical properties profiles across dentin-enamel junction of human incisor teeth. Mater. Sci. Eng. C 2000; 7: 119–128.
15. Staines M, Robinson WH and Hood JAA. Spherical indentation of tooth enamel. J Mater Sci 1981; 16: 2551–2556.
16. Oliver WC and Pharr GM. An improved technique for determining hardness and Young's modulus using load and displacement sensing indentation experiments. J Mater Res 1992; 7: 1564–1583.
17. Lucas BN and Oliver WC. Indentation Power-Law Creep of High-Purity Indium. Metall Mater Trans A 1999; 30: 601-610.
18. Poisl WC, Oliver WC and Fabes BD. The relationship between indentation and uniaxial creep in amorphous selenium. J Mater Res 1995; 10: 2024-2032.
19. Ashby MF and Jones DR (2003). Engineering Materials. 4th ed. Oxford, England: Pergamon Press.
20. Spears IR.A three-dimensional finite element model of prismatic enamel: a re-appraisal of the data on the Young's modulus of enamel. J Dent Res 1997; 76: 1690–7.
21. Katz JL. Hard tissue as a composite material. I. Bounds on the elastic behavior. J Biomechanics 1971; 4: 455-473.
22. Nix WD and Gao H. Indentation size effects in crystalline materials: a low for strain gradient plasticity. J Mech Phys Solid 1998; 46: 41 I-425.
23. Brès EF and Hutchison JL. Surface structure study of biological calcium phosphate apatite crystals from human tooth enamel. J Biomed Mater Res B 2002; 63: 433–440.

List of Tables:

List of Tables:

Figure 6. SEM images of two indents: (a) Cracks initiated from the corners of an indent made by a test with a maximum depth of 500 nm, and (b) No cracks were observed in an indent made by a test with a maximum depth of 2000 nm.

Figure 7. Two extreme loading conditions for an orthotropic composite: (a) Constant-strain condition; and (b) Constant-stress condition.

Figure 8. Upper and lower bounds of the elastic modulus of human enamel over a range of volume fraction of HAP crystallites.

Figure 9. Schematic illustration of the tip-induced realignment of HAP single crystals, as test proceeds and indent depth increases. Note that $\theta_b < \theta_c$.

Table 1: Published data for the hardness and elastic modulus of human enamel measured using indentation method.

Literature	Maximum Depth or Load	Elastic Modulus GPa	Hardness GPa
Willems et al [13]	N/A	90.59±16.13	N/A
Mahoney et al. [12]	N/A	N/A	4.88±0.35
Xu et al. [6]	1.9 N	Occlusal section 98±4 Axial section 86±3	Occlusal section 3.79±0.18 Axial section 3.50±0.12
Cuy et al. [8]	400nm or 800 nm	Axial section Near surface: >115 Near DEJ: <70	Axial section Near surface: >6 Near DEJ: <3
Jiang et al. [9]	1600 uN 300 nm	Axial section 10<E<80	Axial section 0.5<H<5.0
Ge et al. [10]	Prism: 1000uN Sheath 300 uN	Occlusal section Prism: 83.4±7.1 Sheath: 39.5±4.1	Occlusal section Prism: 4.3±0.8 Sheath:1.1±0.3
Habelitz et al. [1]	1500 uN 300 nm	Occlusal section 87.5±2.2 Axial section 72.7±4.5	Occlusal section 3.9±0.3 Axial section 3.3±0.3
Fong et al. [14]	100 nm	Occlusal section 98.3±5.9 Axial section 95.6±4.9	Occlusal section 4.78±0.36 Axial section 4.53±0.26

Figure 1. The hierarchical microstructure in the occlusal section: (a) keyhole-like cross-section of prisms (grey) separated by inter-rod organic sheaths (white); and (b) Each enamel prism is composed of tightly packed fibre-like hydroxyapatite crystallites that are bonded together by a layer of nanometer-thick enamelin. (Courtesy of Habelitz et al.[1])

(a)

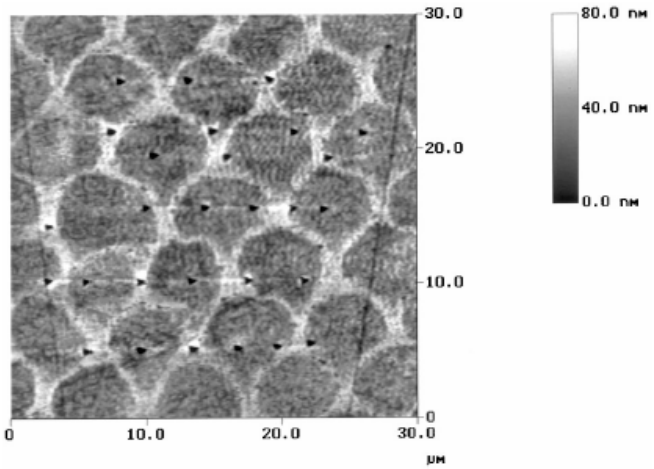

(b)

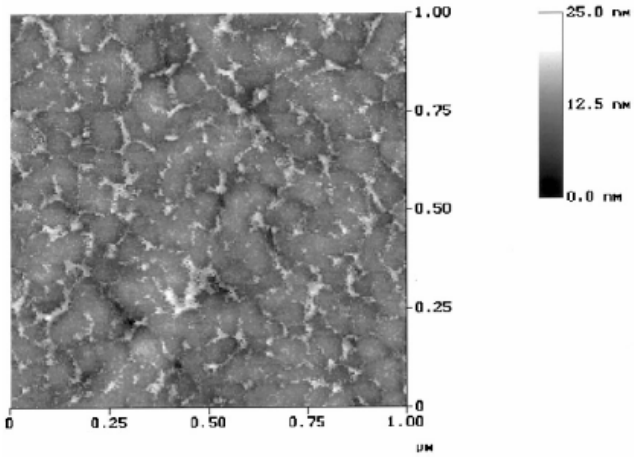

Figure 2. Typical load-depth curves obtained using a target constant strain rate of 0.05 s^{-1}. The two curves represent the load-depth curves of the two sets of tests with the maximum depths of 500 nm and 2000 nm, respectively. Displacement bursts were observed, as indicated by the arrows.

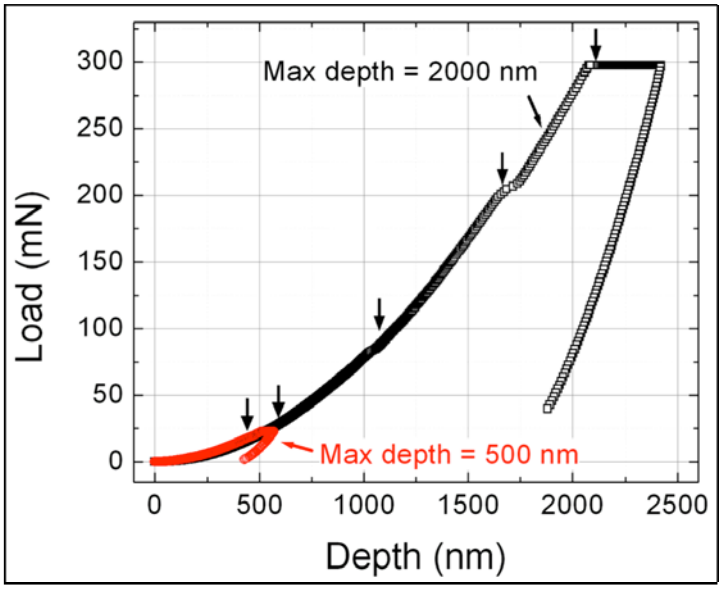

Figure 3. Strain-rate versus indent depth: (a) The two curves correspond to the two load-depth curves that are displayed in Figure 2; and (b) Constant strain rate is reached after the ramping for ~ 100 nm deep for the second set of tests.

(a)

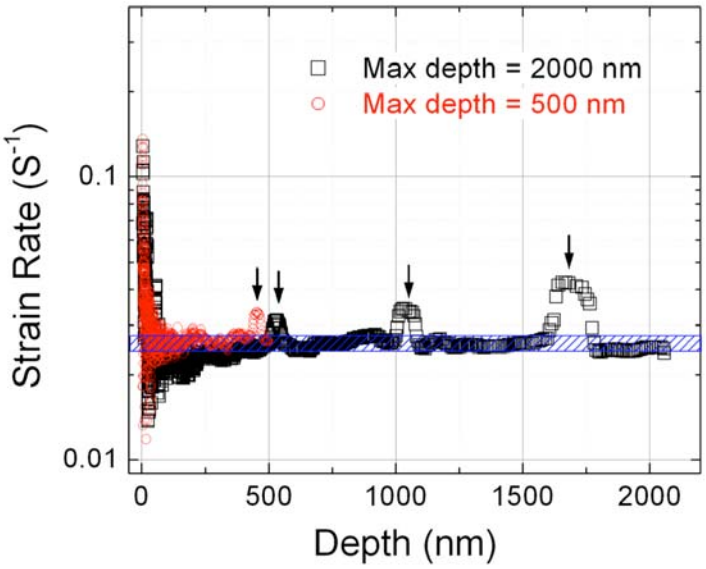

(b)

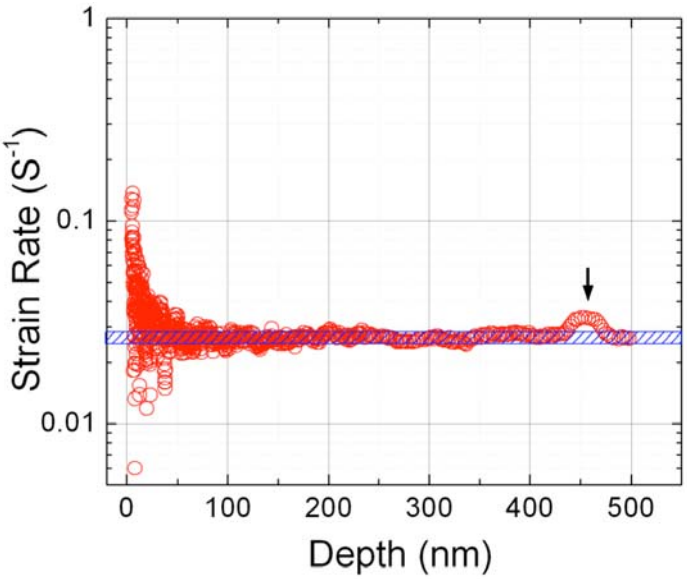

Figure 4: Effects of indent depth on the elastic modulus: (a) Continuous curves; and (b) Plots of the extracted data from the curves in (a).

(a)

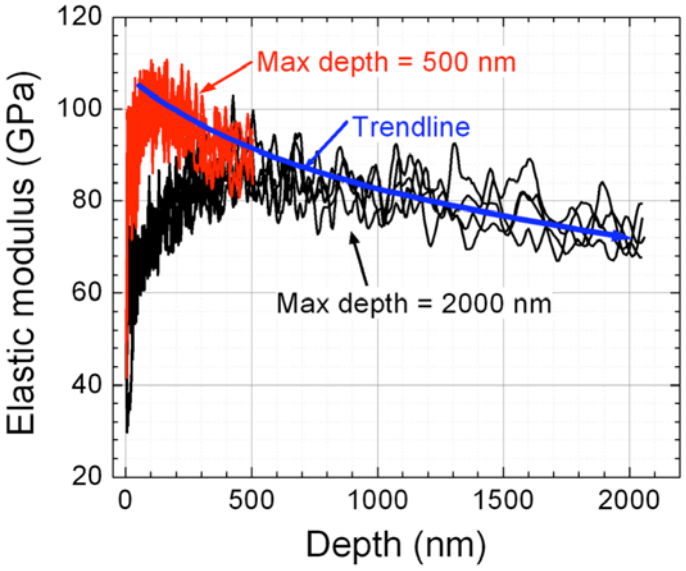

(b)

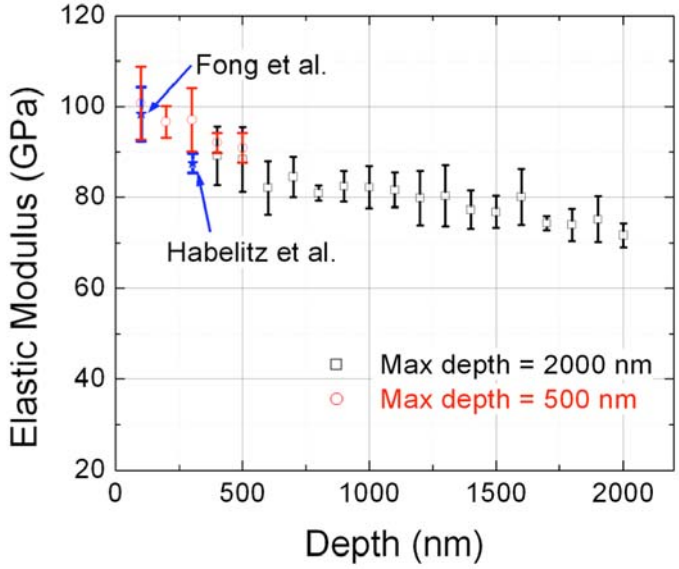

Figure 5. Effects of indent depth on the hardness: (a) Continuous curves; and (b). Plots of the extracted data from the curves in (a).

(a)

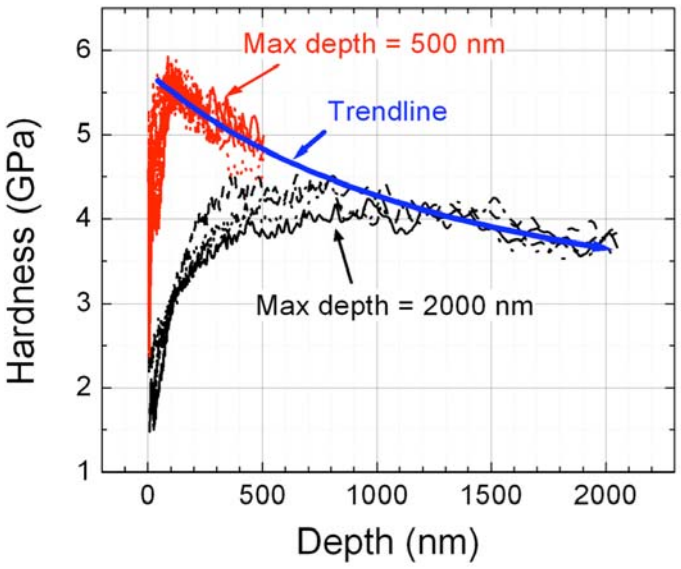

(b)

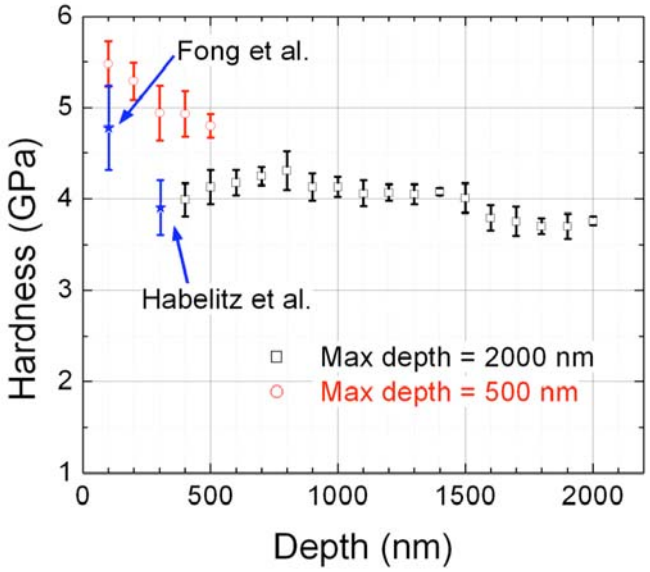

Figure 6. SEM images of two indents: (a) Cracks initiated from the corners of an indent made by a test using a maximum depth of 500 nm, and (b) No cracks were observed in an indent made by a test using a maximum depth of 2000 nm.

(a)

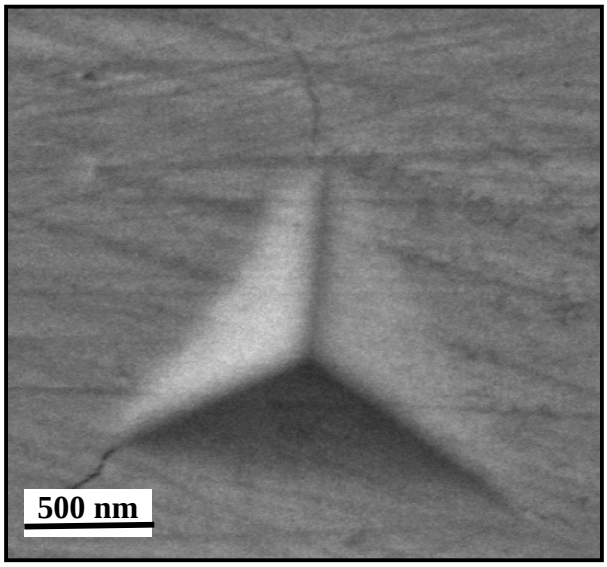

(b)

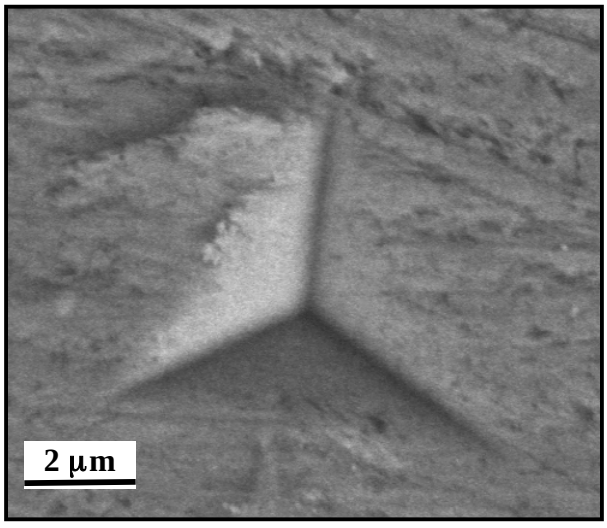

Figure 7. Two extreme loading conditions for an orthotropic composite: (a) Constant-strain condition; and (b) Constant-stress condition.

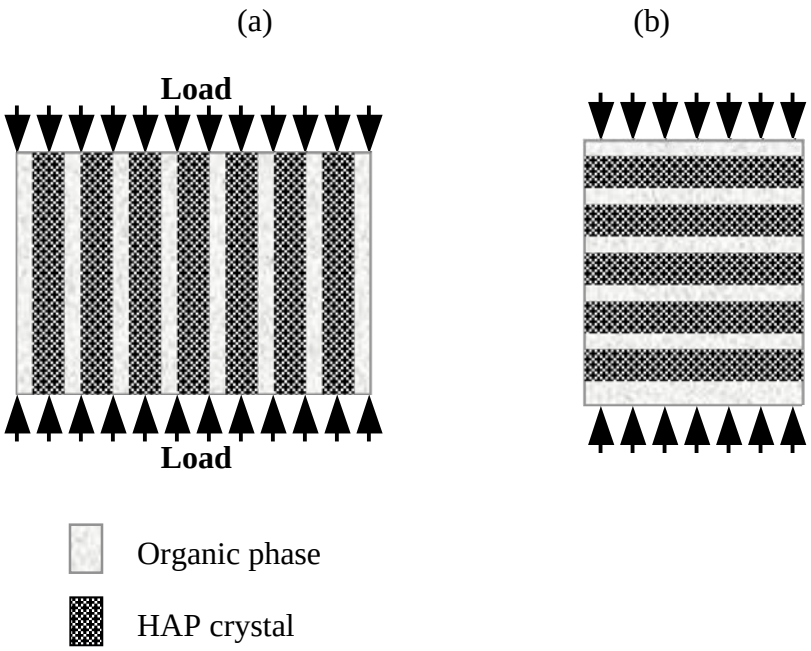

Figure 8. Upper and lower bounds of the elastic modulus of human enamel over a range of volume fraction of HAP crystallites.

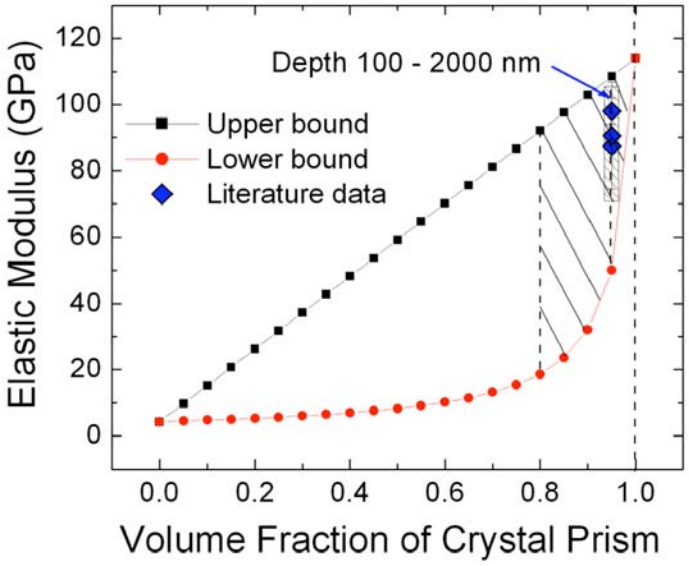

Figure 9. Schematic illustration of the tip-induced realignment of HAP single crystals, as test proceeds and indent depth increases. Note that $\theta_b < \theta_c$.